Enzymatic Degradation of Maize Shoots: Monitoring of Chemical and Physical Changes Reveals Different Saccharification Behaviors

Cécile Barron
INRAE Centre Occitanie-Montpellier: Institut National de Recherche pour l'Agriculture l'Alimentation et l'Environnement Centre Occitanie-Montpellier
Marie-Françoise Devaux
INRAE Pays de la Loire: Institut National de Recherche pour l'Agriculture l'Alimentation et l'Environnement Centre Pays de la Loire
Loïc Foucat
INRAE Pays de la Loire: Institut National de Recherche pour l'Agriculture l'Alimentation et l'Environnement Centre Pays de la Loire
Xavier Falourd
INRAE Pays de la Loire: Institut National de Recherche pour l'Agriculture l'Alimentation et l'Environnement Centre Pays de la Loire
Rachelle Looten
INRAE Pays de la Loire: Institut National de Recherche pour l'Agriculture l'Alimentation et l'Environnement Centre Pays de la Loire
Maud Joseph-Aimé
INRAE Pays de la Loire: Institut National de Recherche pour l'Agriculture l'Alimentation et l'Environnement Centre Pays de la Loire
Sylvie Durand
INRAE Pays de la Loire: Institut National de Recherche pour l'Agriculture l'Alimentation et l'Environnement Centre Pays de la Loire
Estelle Bonnin
INRAE Pays de la Loire: Institut National de Recherche pour l'Agriculture l'Alimentation et l'Environnement Centre Pays de la Loire
Catherine Lapierre
IJPB: Institut Jean-Pierre Bourgin
Luc Saulnier
INRAE Pays de la Loire: Institut National de Recherche pour l'Agriculture l'Alimentation et l'Environnement Centre Pays de la Loire
Xavier Rouau
INRAE Centre Occitanie-Montpellier: Institut National de Recherche pour l'Agriculture l'Alimentation et l'Environnement Centre Occitanie-Montpellier
Fabienne Guillon (fabienne.guillon@inrae.fr)
INRAE: Institut National de Recherche pour l'Agriculture l'Alimentation et l'Environnement https://orcid.org/0000-0001-7925-3104

Research

Keywords: lignocellulosic, plant dry fractionation, recalcitrance, particles size, image analysis, time-lapse study, porosity

Posted Date: September 18th, 2020

DOI: https://doi.org/10.21203/rs.3.rs-73127/v1

Version of Record: A version of this preprint was published on January 5th, 2021. See the published version at https://doi.org/10.1186/s13068-020-01854-1.

Abstract

Background

The recalcitrance of lignocellulosics to enzymatic saccharification has been related to many factors, including the tissue and molecular heterogeneity of the plant particles. The role of tissue heterogeneity generally assessed from plant sections is not easy to study on a large scale. In the present work, dry fractionation of ground maize shoot was performed to obtain particle fractions enriched in specific tissue or molecules. The degradation profiles of the fractions were compared considering physical changes in addition to chemical conversion.

Results

Coarse, medium and fine fractions were produced using a dry process followed by an electrostatic separation. The physical and chemical characteristics of the fractions varied, suggesting enrichment in tissue from leaves, pith or rind. The fractions were subjected to seven hours of enzymatic hydrolysis in a torus reactor designed for real-time monitoring of the number and size of the particles. Saccharification efficiency was monitored by analyzing the sugar content of hydrolysate samples collected at different times. The lowest and highest saccharification yields were measured in the coarse and fine fractions, respectively, and these yields paralleled the reduction in the size and number of particles. The behavior of the positively- and negatively-charged particles of medium-size fractions was contrasted. Although the amount of sugar release was similar, the changes in particle size and number differed during enzymatic degradation. The reduction in the number of particles proceeded faster than that of particle size, suggesting that degradable particles were degraded to the point of disappearance with no significant erosion or fragmentation. Considering all fractions, the saccharification yield was positively correlated with the amount of water associated with [5-15 nm] pore size range at 67% moisture content while the reduction in the number of particles was inversely correlated with the amount of lignin. Lignin could act in maintaining the macroscopic structure of particles without necessarily prohibitive effects on the accessibility of enzymes to their substrates.

Conclusion

Real-time monitoring of sugar release and changes in the number and size of the particles clearly evidenced different degradation patterns for fractions of maize shoot that could be related to tissue heterogeneity in the plant.

1. Background

The development of a plant biorefinery for the treatment of lignocellulosic biomass to produce biomolecules, bioenergy and biomaterials in substitution to fossil carbon is a major challenge today [1]. The biological conversion of cell wall polysaccharides is more attractive than other types of industrial conversion [2] because it offers the possibility to produce specific products with low energy input in an ecofriendly environment. However, with no pretreatment, the conversion yield is low. Many factors are responsible for the recalcitrance linked to both biomass and enzymes [3]. Lignin content is the main component involved in recalcitrance [4, 5]. Other components more specific to grass cell walls, *p*-coumaric acid (CA) end ferulic acid (FA), have been widely investigated in the context of the saccharification performance of grass lignocellulosics [6-8]. Hemicelluloses, and to a lesser extent pectin, are thought to limit cellulose accessibility thereby hindering efficient enzymatic hydrolysis [9-11]. Many pretreatments before the saccharification step aim to reduce the detrimental impact of these components [12]. Cellulose structure, especially crystallinity, has been also linked to saccharification but results have been conflicting [13, 14] or reported little or no effect [15, 16]. At the scale of polymers, the presence of acetyl groups as well as the occurrence of sugar substituents can also limit enzymatic hydrolysis by preventing enzymes from accessing glycosidic linkages (reviewed by [17])

In addition to the influence of the chemical composition of the biomass and of the chemical structure of the constituent polymers, the role of particle size and porosity that determine the surface accessible to enzymes has already been investigated. Conflicting effects of a decrease in particle size on the conversion rates have been reported depending on the substrate, the resulting particle size range or the percentage of fine particles [18, 19]. Several authors, using either solute exclusion [15, 20-23] or Simons' staining [16, 24-26] techniques, reported positive relationships between the internal surface area or pore surface accessible to cellulase and cellulose enzymatic hydrolysis yield and rate. Several methods to investigate the biomass-water interaction have been implemented to explain the recalcitrance phenomenon, including water retention value and time domain low field NMR (LF-NMR). Water retention measures the capacity of the biomass to retain water against a centrifugal force. It has been used as an indirect measure of cell wall properties including overall hydrophilicity and porosity [27, 28] and has been shown to be correlated with saccharification yield [29-31]. LF-NMR relaxometry provides more detailed information on the physical and chemical environment of water in the biomass [26, 29, 30, 32, 33]. This approach revealed that the presence of constrained water favored hydrolysis [30, 33].

To summarize, no real consensus has been reached on the most important causal factors aside from cellulose accessibility and the detrimental role of lignin content. The heterogeneity of the tissues forming the lignocellulosic biomass is also known to cause differences in

saccharification patterns [34]. Several authors have investigated the behavior of different cell types in enzymatic degradation through imaging [8, 35-37] and tissue extraction [38-40]. They demonstrated differences in tissue susceptibility that varied with the nature of the cell walls. Lignocellulosic particles subjected to saccharification originate from different tissues. Anatomical constituents or even tissues could be obtained through dry fractionation [41, 42], which combines grinding and separation processes. Powder enriched in specific anatomical parts of plant is affordable and the initial complexity in bulk samples due to the plant heterogeneity could thus be reduced.

In the present work, it is proposed to separate particles into fractions before saccharification to identify heterogeneity linked to the histological origin of the particles. Maize was chosen as feedstock since it has several characteristics that are suitable for bioconversion. It is mainly grown for the grain so the stalk biomass can be used for biofuel production. Dry fractionation was applied to obtain fractions that differ in their physical state and composition [43]. In addition to the chemical composition of the maize stalks and corresponding fractions, the present work focused on the physical-chemical properties of particles: original particle size distribution, specific surface area, and porosity. NMR techniques were used to evaluate particle porosity, cellulose accessibility and biomass-water interactions at different water contents [26, 30]. A torus reactor prototype designed for image acquisition during the reactions was used for the real-time monitoring of the size and number of particles to identify the effect of physical changes in the particles resulting from the release of sugars during degradation. We hypothesized that measuring both physical and biochemical parameters in contrasting populations of particles would help decipher the mechanisms of the enzymatic reaction.

2. Results And Discussion

2.1. Differences in particle reactivity during saccharification assays of maize shoot powder

First a saccharification assay of the whole maize shoot powder (M) was carried out using the torus reactor Cinetore to analyze the saccharification yield coupled with real time monitoring of changes in the number and size of the particles through image analysis. Before degradation, the maize shoot powder was made of particles of different sizes and shapes (Figure 1a), including long rod-shaped particles. The longest particles were as long as 1,500 µm, (measured by hand).

In the control experiment, the stirring into the reactor caused the disappearance of 19% of the particles and the release of 2.1% of total sugars. This result suggests that some particles were broken down by the mechanical action of the screw and/or the water. After seven hours of saccharification, the number of particles observed was lower (Figure 1b). Changes in the total sum of gray levels relative to time T0 were computed (Figure 1c) to account for the number of particles in the reactor during saccharification. The number of particles rapidly decreased to about 75% after one hour. After seven hours, 26-28% of particles disappeared. In parallel, the amount of sugars released was evaluated from the hydrolysates (Figure 1d). The percentage of disappearance rapidly increased at first and then stabilized at 36-37% after two hours. This result is consistent with results obtained in non-pretreated maize [28]. Clearly, some particles were recalcitrant to enzymatic hydrolysis while others disappeared or were modified.

Changes in particle size during the reaction were also studied. Figure 1e shows the granulometric curves at times T0 and 7 h. The granulometric curves normalized relative to time T0 showed variations both in the number of particles and in the decrease in size. A mode was observed at 90 µm for time T0 and 75 µm for time 7 h. Three size classes were built from these granulometric curves: [0-45 µm], [45-225 µm], [>225 µm]. The three classes represented respectively, 6%, 44% and 50% of the original sample at T0, and 8%, 47% and 45% of the sample after 7 h of hydrolysis. Changes in the number of particles in each class were evaluated after normalization relative to their original number (Figure 1f). A strong relative increase in small particles from 1 to 1.40 and a slight relative increase in medium particles from 1 to 1.06 were observed. In parallel, the number of large particles decreased slightly from 1 to 0.90. Several interpretations are possible. A certain proportion of large, medium, and small particles were fully degraded while others were recalcitrant. Some medium and large particles were degraded and broke into many small particles thereby increasing the relative proportion of small particles. Medium and large particles may be partly eroded during degradation or broken down into medium size particles. Whatever the size, some particles were recalcitrant as small, medium, and long particles were still present after seven hours of degradation. To better understand this heterogeneous behavior, maize shoot powder was sub-fractioned to isolate fractions that were expected to be more homogeneous according to the saccharification process.

1.2. Exploring variability of maize shoot powder

The enzymatic hydrolysis of each particle might be linked to the origin of the tissue in the maize shoot. To explore this hypothesis, dry fractionation was carried out to try to obtain fractions with specific tissue enrichment from leaves, pith, or rind. The particle size obtained in the fractions is not only the result of the efficiency of the grinder but is also due to interactions between plant structures and mechanical loading modes developed in the grinder [43]. The particle size could thus reflect differences in grinding ability in relation to the mechanical properties of

the tissues. On this basis, we chose a separation process mainly based on particle size characteristics [44, 45]. Air classification enabled separation of the original maize shoot powder into three fractions (fine, medium, and coarse). A subsequent step was undertaken to take advantage of differences in particle composition [46]. Electrostatic separation, based on tribocharging, which is an interface phenomenon that depends on surface composition [47],was then used to separate each fraction into two more fractions, giving a final total of six fractions (Figure 2). The coarse, medium, and fine fractions accounted for respectively 43%, 22% and 35% of the weight of the original sample (Table 1). Their median particle sizes (D_{50}) were 310-315 µm, 159-201 µm, and 58-63 µm, for the coarse, medium, and fine fractions, respectively (Table 1). Size dispersion was still observed within each fraction but was less than in the original maize shoot sample, as shown by the narrower range of span values. Electrostatic separation led to no further substantial separation according to particle size, as shown by optical observations (Figure 2) and by laser granulometry (Table 1). The median particle size of samples recovered on the negative electrode side (coded "-") was slightly higher than on the positive ones (coded "+"), in the coarse, medium, and fine fractions. As expected, the reduction in particle size was consistent with an increase in specific surface area measured by physisorption (Table 1). Moreover, the hue of the particles separated by electrostatic separation also differed from the negative fractions with more brownish hues than in the positive fractions.

The chemical composition of each fraction was assessed by focusing on the analysis of the main cell wall components (polysaccharides, lignins, ester-linked *p*-coumaric acid and ferulic acid) that are known to be involved in enzymatic sensitivity. If the total amount of sugars remained relatively stable between the fractions (about 66.7% ± 1.2%), the relative proportion of neutral sugar associated with hemicellulose (arabinose, xylose) was much more variable (relative standard deviation ranged from 8-15%). No major differences in glucose concentrations were observed. Cellulose crystallinity, determined in CP-MAS solid state NMR experiments, was around 25% and no significant difference between fractions was observed. Lignin content, measured using the Klason method, varied significantly from 14.52 to 19.56% in the fractions of cell wall material. Lignin structure was studied by thioacidolysis that estimates the monomer amount of guaiacyl (G), syringyl (S) and *p*-hydroxyphenyl (H) involved in β-O-4 bonds. The thioacidolysis yield ranged from 720 to 999 µmol.g^{-1} KL, suggesting different degrees of lignin condensation in the maize fractions. The S/G ratio of thioacidolysis monomers ranged from 0.9 to 1.42.

Major differences in composition were observed depending on the particle size of the fractions and opposed fine and coarse fractions. The coarse fractions, which could be seen as the most difficult to grind, showed higher concentrations of xylose and Klason lignin and also differences in lignin structure as evidenced by the lower S/G ratio. Lower concentrations of protein, galactose and uronic acid were also observed in the coarse fractions compared to the fine ones. Differences according to the electrostatic separation were also observed: the positively deviated samples ('+') had more acetyl groups, ester-linked *p*-coumaric and ferulic acid, and higher thioacidolysis yields, but lower ash content. Smaller differences were observed between the two coarse fractions compared to between the fine and medium fractions, in particular ash and phenolic acid contents. Electrostatic separation, which is based on surface properties, might be less efficient for bigger particles whose specific surface area is lower [43].

Likewise, particle size fractions isolated from the maize shoot powder differed in chemical composition, supporting the hypothesis that they are enriched in specific tissues. The higher concentrations of galactose and uronic acids in the finest fractions, associated with lower lignin content, suggests enrichment in pith from the stem [48]. However the higher amount of ash, also expected in this case [49], was not observed in this sample set. Leaves were also expected to be more present in the finest fractions [45]. In Poaceae, compared to the stem, leaves are characterized by less xylose and more protein, like in sorghum [50], more ash [51, 52], a lower S/G ratio, like in sugarcane, and less ester-linked *p*-coumaric [52]. More leaves in the fine fraction can be assumed from lower xylose or higher protein amounts. The fine fractions were found to be the richest in lignin syringyl units (%S > 55%), despite their lower lignin content. This observation suggests that these fractions are enriched in leaf blade sclerenchyma, a tissue repeatedly shown to contain lignins rich in S units [34, 53]. In negatively deviated fractions ('-'), an enrichment in ash was observed combined with a brownish hue (Figure 2). This could reflect more leaves, even if protein enrichment was not that high. Nevertheless, based on our compositional analysis, we propose the following interpretation: coarse fractions could originate from the stem rind, while the fine fractions could be enriched in pith and leaves. The enrichment in leaves may also differ according to the electrostatic separation, with more leaves in the M*f-* fraction. Medium fractions could contain tissues from both origins, again with more leaves in the M*m-* fraction.

1.3. Degradation kinetics by imaging and chemical analyses: Cinetore experiments

The parallel release of sugar and changes in the number and size of the particles during saccharification was analyzed in Cinetore experiments. The coarse fraction considered corresponded to the whole M*c* fraction (obtained before electrostatic separation) as the compositions of the two fractions M*c- and* M*c+* were close.

1.3.1. Fractions at time T0

Examples of images at time T0 are given in Figure 3 for the five fractions. Although the same mass of particles was loaded in the reactor, the images of particles differed considerably. At T0, particles in M*c* were mainly elongated with variable thickness and length. As expected, particles in the medium fractions (M*m*+ or M*m*-) were clearly more numerous and differed in shape: thin and elongated to almost isotropic and cuboid shapes. In the raw images (see Additional file 2), particles in the fine fractions (M*f*+ or M*f*-) were so numerous that they could hardly be distinguished. Considering the D_{50} measured by laser granulometry (60 µm) and the pixel size (8.2 µm), only a few pixels are required to observe one particle and their overlapping led to a low contrast between background and particles. The bright background attested to the high density of particles and to particles smaller than the pixel size. After subtracting the background (Figure 3), many isotropic particles were observed together with small pointed particles and a few elongated particles. For these fine fractions, the estimation of the relative number of particles from the total gray levels would be underestimated and should be considered relative to the number of particles larger than 8.2 µm.

For the fine fraction, the mode was found at 55-75 µm while it was 90-125 µm and 155-205 µm for the medium and coarse fractions, respectively. The mode corresponded to the D_{50} (Table 1) in the case of the fine fractions and was lower for the other fractions. It should be noted that particle size evaluated by image analysis is more sensitive to the smaller dimensions of the particles [54], i.e. the width rather than the length, compared to laser granulometry. In addition, the variations in gray level observed for large sizes in the case of fine fractions were caused by the overlapping of the numerous particles. To a lesser extent, variations in gray level were observed for small sizes in the medium and coarse particles, which actually corresponded to irregularities in their contour.

1.3.2. Changes in the number and size of particles during saccharification

After seven hours of saccharification (Figure 3), particles could still be seen in the images, regardless of the fraction concerned. Fewer particles were observed in the coarse fraction M*c*, and the contrast was lower. In the fine fractions, the contrast was lower after seven hours compared to T0 and fewer particles could be distinguished. A decrease in the number of particles was also visible in the medium fractions. Considering the gray level granulometric curves normalized with respect to time T0, the lower intensity of the curves clearly confirmed the decrease in the number of particles in all the fractions, with the biggest decrease in the fine (M*f*-, M*f*+) and M*m*- fractions. In the fine fractions, a decrease in particle size was evidenced with an absolute increase in the number of particles smaller than 25 µm, whereas a moderate decrease in particle size was observed in the coarse and medium fractions.

To investigate physical changes in the particles depending on the period of saccharification in more detail, the number of particles was deduced from the total amount of gray levels, and mean particle size was estimated from the gray level mean sizes (Figure 4a and 4b, respectively). In all the fractions except M*c*, the decrease in the number of particles was always greater than the decrease in particle size. The kinetics were analyzed through the time needed to obtain a 50% reduction in the number of particles or in their size ($t_{1/2}$): in most cases the reduction in the number of particles took place more quickly than the reduction in particle size.

The least change in the number and size of particles was observed in the coarse fraction M*c*. The total decrease in gray levels between images after seven hours of degradation was 12% and the gray level mean size decreased by 8%. The size and number of particles decreased with quite similar $t_{1/2}$ ($t_{1/2}$ = 1.08 h and 0.82 h respectively).

Conversely, the fine fractions (M*f*+ and M*f*-) were the most impacted during saccharification: after 7 h, the total decrease of gray levels was 36% and 32% in M*f*+ and M*f*, respectively, and the gray level mean size also decreased by 20% and 17% in M*f*+ and M*f*-, respectively. For the sake of comparison, the decrease in the total gray level in the control experiments was 28% and 18% in M*f*+ and M*f*-, respectively. Particle disappearance was clearly enhanced by enzymatic hydrolysis. The size and number of particles varied consistently with a rapid and important decrease occurring in the first 15 min. These two phenomena were observed following similar kinetics in the M*f*+ fraction, whereas in the M*f*- fraction, the decrease in particle size was slightly slower ($t_{1/2}$=19 min) than the decrease in the number of particles ($t_{1/2}$=10 min).

Different patterns were observed in the medium fractions. In M*m*- samples, after seven hours of saccharification, almost no significant change in particle size (9%) was observed, while the number of particles decreased by about 34%. Mechanical stirring alone could not explain such a discrepancy as the gray level decrease in control experiments was only 4%. This result suggests that saccharified particles were fully dissolved in the aqueous medium with no noticeable particle erosion or breaking. The reduction in the total number of particles was similar to that obtained in the fine fractions but was less rapid ($t_{1/2}$ = 49 min for M*m*- compared to $t_{1/2}$ = 10 min and $t_{1/2}$ = 7 min for M*f*- and M*f*+, respectively). This could suggest similar tissue composition but differences in surface accessibility (in relation to particle size) between M*m*- and fine particles. In the M*m*+ sample, the particle size reduction was also very small (10%) but the reduction in the number of particles was also smaller (20-24%). Particle changes in M*m*+ were the slowest observed in these fractions, as indicated by the higher values of $t_{1/2}$ (around 2.5 h). The reduction in both the number and size of the particles were moderate, even less than in the coarse fractions during the first 90 min.

Differences in the physical change pattern were next observed according to particle size. Fine particles were the most impacted, regardless of the criteria used (number of particles or size), the coarse ones the least. Concerning the disappearance of particles, the medium fractions were

between the two but concerning the decrease in particle size, their behavior was closer to that of the coarse fraction.

1.3.3. Sugar release during saccharification

After seven hours of hydrolysis, sugar release was 22%, 34%, 38%, 52% and 55% in M*c*, M*m*-, M*m*+, M*f*-and M*f*+, respectively (Figure 4c). The main differences were observed according to the overall particle size of the fraction, with coarse, medium, and fine fractions ranked according to increasing hydrolysis yield. Concerning electrostatic separation, the medium and fine fractions obtained at the positive electrode were slightly more degraded than those recovered at the negative electrode.

Concerning kinetics, the saccharification of the fine fractions was the most rapid as shown by the lowest $t_{1/2}$ (around 6 min), while the coarse fraction had the highest $t_{1/2}$ value (10.4 min). As suggested by Mansfield et al. [55], the smallest size fractions were hydrolyzed preferentially during the first stage of the hydrolysis reaction. Contrasted kinetic values were observed for medium fractions: saccharification of M*m*+ was as slow as in the coarse fraction ($t_{1/2}$ =10.1 min) whereas M*m*- behaved like the fine fraction M*f*-.

1.3.4. Coupled physical and chemical changes during saccharification

Saccharification was described by combining the analysis of saccharification yield, the reduction in the number and size of particles (Figure 5). Whatever the fraction, the maximum relative change in the number of particles (dotted lines) was still lower than the chemical saccharification yields obtained at the plateau. The times to reach 50% of the modification were always shorter for chemical changes than for physical changes. This result suggests that at least some particles were fully degraded, as evidenced by the decrease in the total number of particles, while other particles were only partially degraded. Sugar release could be mainly due to the hydrolysis of few particles potentially originating from highly hydrolysable tissues, such as pith parenchyma [8] or leaves [56].

1.4. Relationships between physicochemical characteristics, water mobility distribution and saccharification patterns

High sugar release prior to the reduction in the number and size of the particles, observed particularly in the M*m*+ fraction, could be explained by the open porosity of the particles. The specific surface (Ssp) area of all the fractions measured by physisorption was systematically higher than the Ssp area calculated from granulometric curves (Figure 6), also supporting the presence of open porosity at mesoscale (2-50 nm pore size). A high correlation (R^2 = 0.915) was observed between the values obtained with the two methods. M*m*+ did not deviate from this relationship (Figure 6). However, the specific surface area measured by physisorption corresponded to the surface area available to krypton molecules and but not to the surface accessible to cellulase, whose mean size is about 5.9 nm [57]. Moreover, values were determined in dry state at -195.8 °C, quite far from hydrolysis conditions implying swollen substrates.

Swelling properties and water retention capacity (WRC) whose values include both water at the surface and between the particles and water within the biomass were considered (Table 3). The coarse fractions had the lowest values for both swelling and WRC, and the fine fractions the highest. A positive correlation was found between these properties (in particular swelling capacity) and sugar release (R^2=0.915) and the reduction in particle size (R^2=0.968) after seven hours of saccharification. However, here again, M*m*+ did not differ from M*m*- and their values were intermediate between those of the coarse and the fine fractions (Table 3). Differences in swelling and WRC did not reflect the specific saccharification pattern of the M*m*+ fraction.

Low-field nuclear magnetic resonance (LF-NMR) was used to obtain information on water-biomass interactions at the molecular-scale. relaxation times of water proton distribution and their relative proportions were determined. To take advantage of the high sensitivity of this approach to any changes in sample supramolecular structure associated with water distribution and diffusion specificities, water-fraction interactions were investigated at five different moisture contents (MC) ranging from 15% to 67%. It should also be noted that at low water content (15% MC), the NMR signal is expected to be dominated by water arising from the hydration shell of macro-molecules and from water in interaction within the small pores of matrices, reporting on their microstructural specificities.

As illustrated in Figure 7, the analysis of relaxation curves led to profiles with multiple distinct peaks. Because no simple direct relationship exists between components and the morphological compartments in biological tissues [58], each peak can be preferentially assigned to a pool of water at a given range of mobility corresponding to specific molecular environment/interactions. Both the number of components, the relative surface area, and the individual mean relaxation time values associated with these peaks changed with increasing water concentration and differed between the five fractions M*c*, M*m*-, M*m*+, M*f*- and M*f*+. Overall, increasing moisture content led to an increase in the number of components (from 1-2 at 15% MC to 5-6 at 67% MC) with, in most cases, a shift towards higher water mobility modes, which could partially

result from swelling. However, it should be noted that a short mode, centered around 2 ms, was present from 40% to 67% MC with only small changes in value/mobility, indicating that the physical-chemical environment associated with the highly constraint water molecules can remain relatively unaffected in this range of moisture contents. In any case, differences between profiles of maize fractions were observed (Figure 7), regardless of the particle size, the electrostatic deviation, and the water content.

The water content associated with the [5. 15[pore size range (in nm) that typically represents the average diameter of enzymes, was investigated in more detail (Figure 7, shaded area). The water content associated with this pore size range at 67% MC was positively correlated with the saccharification yield (R^2 = 0.881) (Figure 8). It was also correlated with the water content associated with pore sizes below 4.3 nm at 15% MC (R^2=0.992). At 15% MC, the profiles of the five fractions showed two peaks with short relaxation times (≤ 4.3 ms). The population , associated with the component, was positively correlated with specific surface area (Figure 9-a, R^2=0.969), suggesting that this component is mainly influenced by water molecules located at the surface of particles. The of M*m*- fraction was of the same order as that of the fine fractions, whereas the value measured for M*m*+ was between the fine and coarse ones. Therefore, M*m*- differed from M*m*+ by more constrained water, which is hypothesized to be essentially located at the surface of particles. Despite the very small change in the shortest relaxation time value, it proved to be positively correlated with lignin content (Figure 9-b, R^2 = 0.983). This could mean that the hydrophobic character of lignin may induce an increase in water mobility, in turn resulting in an increase in the relaxation time centered from around 1.10 ms to 1.35 ms. The M*m*+ fraction, with its higher lignin content, could keep the same macroscopic structure while still allowing accessibility to sugar hydrolysis.

Even at low moisture content, water/fraction interactions could be related to sugar release. The decrease in the number of particles was negatively correlated with the shortest centered around 1.2 ms observed at 15% MC (Figure 9b; R^2 = 0.990) and the lignin content (R^2 = 0.983). Moreover, the population , associated with the component, was positively correlated with the reduction in mean particle size (Figure 9a; R^2 = 0.982). Thus, these two relaxometric parameters (and) could be early (at low MC) indicators of the saccharification potential, particularly when no significant swelling of the biomass matrix has yet occurred.

3. Conclusion

Dry fractionation of plant biomass based on particle density and electrostatic properties produced fractions with different chemical composition and physical-chemical properties, which may reflect variations in the relative proportions of tissues originating either from the stem or the leaves. Real-time monitoring of sugar release under the action of enzymes and changes in the physical state of the particles clearly evidenced different degradation patterns for these fractions. The sugar release could be related to specific surface area, swelling, and the amount of water associated with pore size [5-15 nm] at 67% relative humidity, which represents the zone of accessibility to enzymes. Changes in particle size and in the number of particles were more complicated to interpret. They were not necessarily synchronous with sugar release. Furthermore, the relative decrease in particle size was much smaller than the relative decrease in the number of particles. This suggests that (i) there were different populations of particles within the fractions: recalcitrant and degradable particles, (ii) concerning the degradable particles, chemical degradation may occur inside the particle with no visible change in particle size to a point where the weakened particles break and then degrade rapidly and completely. The decrease in the number of particles during the course of the enzymatic reaction, or in other words, the disruption of particles up to their disappearance, was inversely correlated with the amount of lignin. Thus, lignin does not necessarily hinder the access of enzymes to the cell wall polysaccharides but may preserve the macroscopic structure of the particle despite high sugar release.

4. Materials And Methods

4.1. Materials

The maize variety Maxxis was harvested at the silage stage. The maize shoot, i.e. without ears but containing both stems and leaves was oven dried at 55 °C and ground with a hammer mill with a 1-mm screen.

The whole ground maize shoot was separated into three fractions (coarse '*c*', medium '*m*' and fine '*f*') based on particle size using an air classification process (Hozokawa Alpine 50 ATP turboplex). The air classifier wheel was first set at 2,500 rpm rotor speed to collect the coarse fraction and the remaining fraction was then separated into medium and fine fractions with the rotor speed set at 4,000 rpm. Each fraction was further separated electrostatically (TEP System, Tribo Flow Separations, Lexington, U.S.A). Two fractions were recovered, one on the negative electrode side (coded "-") containing the positively charged particles, one on the positive one (coded "+"), containing negatively charged particles. Particles in bulk were observed using the AZ100M Multizoom (Nikon, Japan) using white LED epi-illumination at low magnification (x4).

4.2. Physical-chemical characterization

Except for particle size analysis, measurement of specific surface area and lignin composition, all the experiments were carried out on water insoluble material. About 1 g of sample was suspended in 200 mL of distilled water containing 0.02% merthiolate (by weight). The suspension was stirred overnight at 40 °C, and then filtered through a 10 µm nylon filter cloth. The insoluble fractions were washed with 50 mL of distilled water and then freeze dried.

1.2.1. Particle size analysis

The particle size distribution of the maize shoot fractions was measured using a Mastersizer 2000 laser diffraction particle size analyzer (Malvern Instruments Ltd., United Kingdom). Measurements were taken in ethanol, using 40% ultrasound power and setting obscuration at between 10% and 20%. Median diameter (D_{50}), span ($(D_{90}-D_{10})/D_{50}$) and the calculated specific surface were extracted from particle size distribution expressed in volume from at least three parallel analyses per sample. The parameters D_{10}, D_{50}, and D_{90} indicate that respectively 10%, 50%, and 90% of the particles examined were below the corresponding diameter expressed in µm. The span represents the width of the particle size distribution.

1.2.2. Specific surface measurement

The Kr adsorption isotherms were determined using an ASAP 2460 (Micromeritics, France) at -195.8 °C. Samples (approx. 1 g) were first degassed under vacuum at 50 °C for 48 h (VacPrep 061, Micromeritics, France). The specific surface area was deduced from the Branauer-Emmett-Teller fitting method of isotherm at a partial pressure of between 0.02 and 0.3, and the mean relative deviation between duplicates was less than 3%. The measured surface area accounted for the whole rough external surface and for the surface accessible in the open porosity at mesoscale (2 nm-50 nm pore size).

1.2.3. Swelling capacity

The swelling capacity of the powdered samples was measured using the bed volume technique [59]: 100 mg of sample was dispersed in 10 mL of distilled water in a graduated cylinder and left overnight at room temperature. The volume of the swollen sample was then measured and expressed as mL of swollen sample per g of original dry sample.

1.2.4. Water retention capacity (WRC)

WRC was evaluated as the capacity of powder to hold water against a centrifuge force as described by Guillon et al. [60]. Three hundred mg of sample were suspended in 25 mL of deionized water and allowed to settle overnight at 4 °C under gentle stirring. The suspension was then centrifuged at 3,000 g for 20 min at 20 °C and the supernatant was eliminated by passing the sample through a filter (mesh size 100 µm). The pellet was transferred to a weighed sinter (G2) to drain for 2 h. Sample fresh weight was recorded prior to drying at 103 °C overnight. The WRC was deduced from the water retained in the pellet divided by the sample dry mass. The mean relative deviation between duplicates was less than 4%.

1.2.5. Water mobility and pore size distributions

Water mobility and pore size distributions were measured by low-field nuclear magnetic resonance (LF-NMR) relaxation. Each fraction was left at controlled humidity (0.98 a_w) for different times to reach the same moisture content (ranging from 15-67%).

LF-NMR analyses were carried out using a Minispec mq20 spectrometer (Bruker) operating at 0.47 T (20 MHz proton resonance frequency) equipped with a thermostated (± 0.1 °C) ^{1}H probe. Fractions were packed in a 10-mm-diameter NMR tube to reach 1 cm in height and left for 10 min in the spectrometer for the temperature to stabilize at 4°C. The transverse relaxation curves were acquired using a Carr–Purcell–Meiboom–Gill (CPMG) sequence. The 180° pulse separation was 0.2 ms, 1,024 even echoes were collected, and 2,048 scans were acquired with a recycle delay of 0.5 s resulting in a total acquisition time of about 20 min.

After acquisition, water was added to successively reach a hydration level of about 27%, 39%, 53% and 67%, and an interval of four days was left before the following measurements. The number of even echoes collected (2,048 to 20,000), the number of scans (1,024 to 128, respectively) and the recycle delay (from 1 to 5 s) were adjusted for each hydration state (from 27% to 67% w/w).

An inverse Laplace transformation (ILT) was applied to convert the relaxation signal into a continuous distribution of the relaxation components. For this purpose, a numerical optimization method was used by including non-negativity constraints and L1 regularization and by

applying a convex optimization solver primal–dual interior method for convex objectives (PDCO) [61, 62]. Similar NMR acquisition and data treatment protocols were implemented on controlled pore glass samples of known diameters (Sigma Aldrich; pore size: 8, 25, 50 and 100 nm). A linear relationship (R^2 = 0.998) between values and pore diameter was thus established and used to convert distributions of biomass fragments into pore size distribution.

4.2.6. Cellulose crystallinity

NMR experiments were performed on a Bruker AvanceIII-400 MHz spectrometer operating at a ^{13}C frequency of 100.55 MHz and equipped with a double-resonance H/X CP-MAS 4-mm probe for CP-MAS solid-state experiments. Experiments were carried out at ambient temperature (20 C). Contact time was 1.5 ms. A typical number of 3,072 scans was acquired for each spectrum. Chemical shifts were calibrated with external glycine, assigning the carbonyl carbon at 176.03 ppm. To determine the degree of crystallinity of cellulose, the 78-90 ppm region of ^{13}C spectra was decomposed as previously described [63] using Peakfit® software.

4.2.7. Chemical composition

Except for lignin measurements, all analyses were carried out on water insoluble material. Lignin analyses were performed on extractive free material. Extractive-free material was prepared by exhaustive extraction with water and ethanol before drying at 40 °C. All the analyses were performed in duplicate except for uronic acid and ash content determined in a single test.

Neutral sugars were analyzed by gas chromatography (GC) after sample hydrolysis by sulfuric acid conversion of the monomers to alditol acetates as previously described [63]. The mean relative deviation between duplicates was less than 5%. Total neutral sugars in enzymatic hydrolysates were quantified using the colorimetric orcinol method [64] with glucose as standard. The uronic acid content in the sulfuric acid and enzymatic hydrolysates was determined using the metahydroxydiphenyl colorimetric method [65] and glucuronic acid as standard. The total amount of proteins was estimated using the Kjeldahl method with a nitrogen protein conversion factor of 6.25. The mean relative deviation between duplicates was 25%. Acetyl contents were measured by HPLC after alkaline hydrolysis according to [66] and the mean relative deviation between duplicates was less than 6%. Ash content was measured using the thermogravimetric method according to the standard NF EN ISO 2171 (2010).

Ester-linked *p*-coumaric and ferulic acids were measured after mild alkaline hydrolysis [67], with a mean relative deviation of 2% between duplicates.

Klason lignin content was measured according to Dence [68]. Lignin structure was investigated by thioacidolysis [69]. Lignin-derived monomers were analyzed via their trimethylsilyl derivatives by gas chromatography-mass spectrometry (GC-MS). The mean relative deviation between duplicates was less than 2%.

4.3. Saccharification experiments

4.3.1 Enzymes

The three commercial preparations, *Trichoderma reesei* cellulase (NS50013), β-glucosidase (NS 50010) and xylanase (NS 55030) were gifts from Novozymes (A/D Bagsvaerd, Denmark) and were used in combination for saccharification tests. Prior to use, the enzyme preparations were desalted on a PD-10 column (GE Healthcare Bio-Sciences AB, Uppsala, Sweden) to remove low molecular weight stabilizers. The main activities of the desalted preparations were determined on model substrates (Additional file 1).

4.3.2 The torus reactor Cinetore

Maize fractions were evaluated for saccharification kinetics in a torus reactor prototype named ‘Cinetore’ equipped for the visualization of particles at the macroscopic scale [70]. It is pictured in Figure 10. The reactor is a steel block in which half a torus was machined. The diameter of the torus is 100 mm and the semi-circular section is 25 mm, giving a total volume of 205 mL. The geometry of the torus was distorted to allow the visualization of particles while maintaining a constant section volume. The reactor is closed by a transparent polycarbonate cover including a neutral video filter (r = 25 mm) as visualization window. The background of the steel block under the visualization window was painted black. Forty-eight green leds (525 nm Agilent HLMP-CM36-X10xx) were enclosed in the steel block around the visualization window at an angle of 30° to provide diffuse lighting of the samples through the particles. Particles therefore appear as bright objects against a black background. The Cinetore reactor was equipped with a monochrome camera (PROSILICA EC1600, Alliance Vision, Montélimar, France) that

allows the acquisition of 1,220 x1,620 pixels monochrome images with gray levels coded between 0 (black) and 255 (white). Flat resistances glued under the steel block and a thermocouple probe enabled the temperature inside the reactor to be controlled. Stirring is ensured by a three-blade screw driven by a variable speed motor. The reactor was placed in a vertical position with an opening at the top to allow the medium to be sampled for chemical analysis. A x0.55 telecentric lens (T100/0.6 Vision Control, Alliance Vision, France) was used: the pixel size was 8.2x8.2 µm², and the field of view 10.0x13.3 mm².

4.3.3 Hydrolysis experiment

Four hundred mg of water insoluble material was suspended in water and placed in the Cinetore reactor. The volume was completed to 200 mL with deionized water. Degradation took place at 40 °C for a period of seven hours in the presence of an enzymatic cocktail. Enzymes were added at a proportion of 18, 2.4, and 1.7 mg of proteins/100 mg of dried fraction for cellulase, endoxylanase, and glucosidase, respectively. Experiments were performed in duplicate. In addition, one control experiment was performed with no enzyme.

The suspension was stirred throughout the reaction and the particles moved continuously inside the reactor. During the saccharification process, images of the particles were automatically acquired at 0, 5, 10, 15, 20, 25, 30 and 45 min, 1 h, 1 h 30, 2 h, 2 h 30 and 3, 4, 5, 6 and 7 h. Ten images were recorded on each occasion.

The chemical degradation of particles was evaluated by measuring the amount of sugars solubilized. Hydrolysates were sampled at times 0, 15, 30, 45 min, 1, 2, 3, 5, and 7 h. The hydrolysates were boiled for 10 min to inactivate the enzymes, centrifuged for 5 min (8,500 rpm, Sigma 6K10). Concentrations of uronic acid and neutral sugars in the supernatants were measured using colorimetric methods. The amount of sugar released at each measurement time is expressed as % of the total sugars in the original material (T0).

The kinetics of sugar release were modeled with an exponential law (one or two exponentials, depending on the fraction considered) to evaluate asymptotic values and, in particular, to extract the parameter $t_{1/2}$, defined as the time necessary to obtain 50% of the full range of variation.

4.3.4 Image analysis

Image preprocessing

Examples of raw and preprocessed images are provided in Additional file 2 in which the particles appear as bright objects against a dark background. The general background of images changed during enzymatic degradation. Background variations were removed using the *tophat* transformation from mathematical morphology [54]. The *tophat* transformation selects bright objects smaller than a mask of a given shape and size called *structuring elements*. In the present work, a squared structuring element was considered with a side measuring 131 µm corresponding to 1,075 µm.

Number of particles

The total number of particles was evaluated as the sum of gray levels of preprocessed images at time T0. The values of the 10 images acquired at T0 were averaged to obtain the original value. The decrease in the number of particles during the reaction was measured as the percentage of relative decrease with respect to the original values. Again, values of 10 images acquired at each measurement time were averaged.

Particle size evolution

A huge number of particles was observed in the images making individual particle identification irrelevant (Figure 1). Particle size evolution was therefore evaluated overall from the total particle population with no segmentation steps. Gray level granulometry based on mathematical morphology tools was used for this purpose [54]. It was applied as described by [70, 71]. The method provides granulometric curves that can be compared to usual granulometric distributions except that they are based on measurements of variations in the gray level. The technique does not extract the so called “actual size distribution” but enables comparison of images in a given experiment. Mean sizes can be calculated from the granulometric curves that were called “gray level mean size” [71].

In the present work, granulometric curves were computed using *morphological opening* by *linearstructuring elements* [54] to account for the fact that many particles were elongated. Because of the random orientation of particles in the images, two orientations of the structuring elements (0 and 90°) were applied. Granulometric curves therefore measured the distribution of the average projected length of particles at 0 and 90°. The maximum size analyzed was 1,075 µm with a 16.4 µm step between two sizes. The 0 and 90° granulometric curves of the 10 images acquired at a given time were averaged to obtain a single granulometric curve per measurement time.

Granulometric curves are usually normalized with respect to the total gray levels of the image considered, i.e. the total number of particles in the image. In the present work, a second kind of normalization was used for the total gray levels of the image at time T0 for all images of a given kinetic, i.e. the total number of particles in the original image at time T0.

Gray level granulometric curves were computed using homemade software developed with Matlab and available at http://www.pfl-cepia.inra.fr/index.php?page=granulomorphogui_en).

Abbreviations

D_{50} median diameter of particle size distribution expressed in volume

FA ferulic acid

CA para-coumaric acid

Ssp specific surface area

WRC water retention capacity

MC Moisture content (wet basis)

Declarations

Ethics approval and consent to participate

Not applicable

Consent for publication

Not applicable

Availability of data and materials

The datasets used and/or analysed during the current study are available from the corresponding author on reasonable request.

Competing interest

The authors declare that the research was conducted in the absence of any commercial or financial relationships that could be construed as a potential conflict of interest

Funding

This work was supported by grants from INRAE (AIC Histochem and AIC Apsali) and funds from the EU Framework programme 7, project 211982 (RENEWALL).

Author Contributions Statement

Composition and physicochemical characterization: LS, EB, CL, MJA, FG, CB, SD

Cinetore experiments: RL, FG, MFD

NMR relaxometry experiments: LF, XF

Dry fractionation of maize shoot: CB, XR

Image analysis and chemometrics: MFD, CB, LF

Data interpretation: CB, MFD, LF, XF, RL, MJA, SD, EB, CL, LS, XR, FG

Experimental design: FG, CB, MFD, XR

Manuscript writing – original draft: CB, FG, MFD, LF

Manuscript writing – review and editing: CB, MFD, LF, XF, RL, MJA, SD, EB, CL, LS, XR, FG

Acknowledgments

The authors acknowledge Y. Mellerin and G. Maraval for their technical assistance in maize shoot fractionation experiments and particle size distribution measurements and the platform for Processing of PLANt product with Emergent Technologies of the JRU IATE for its support (PLANET, doi: 10.15454/1.5572338990609338E12). We are indebted to Laurent Cézard and Fréderic Legée for their technical assistance with lignin analyses. The authors thank A. Sire and P. Papineau who designed and built the torus reactor CINETORE. NMR analyses were performed at the INRAE BIBS facility, F-44316 Nantes.

References

1. Isikgor FH, Becer CR. Lignocellulosic biomass: a sustainable platform for the production of bio-based chemicals and polymers. Polymer Chemistry. 2015;6(25):4497-559.
2. Menon V, Rao M. Trends in bioconversion of lignocellulose: Biofuels, platform chemicals & biorefinery concept. Progress in Energy and Combustion Science. 2012;38(4):522-50.
3. Foston M, Ragauskas AJ. Changes in the Structure of the Cellulose Fiber Wall during Dilute Acid Pretreatment inPopulusStudied by1H and2H NMR. Energy & Fuels. 2010;24(10):5677-85.
4. Dien B, Jung H, Vogel K, Casler M, Lamb J, Iten L, et al. Chemical composition and response to dilute-acid pretreatment and enzymatic saccharification of alfalfa, reed canarygrass, and switchgrass. Biomass and Bioenergy. 2006;30(10):880-91.
5. Jung HJG, Bernardo R. Comparison of Cell Wall Polysaccharide Hydrolysis by a Dilute Acid/Enzymatic Saccharification Process and Rumen Microorganisms. Bioenerg Res. 2012;5(2):319-29.
6. Grabber JH, Hatfield RD, Ralph J. Diferulate cross-links impede the enzymatic degradation of non-lignified maize walls. J Sci Food Agric. 1998;77:193-200.
7. Grabber JH, Hatfield RD, Ralph J, Zon J, Amrheins N. Ferulate cross-linking in cell walls isolated from maize cell suspensions. Phytochem. 1995;40(4):1077-82.
8. Jung HG, Casler MD. Maize stem tissues: Impact of development on cell wall degradability. Crop Science. 2006;46(4):1801-9.
9. Hu J, Arantes V, Saddler JN. The enhancement of enzymatic hydrolysis of lignocellulosic substrates by the addition of accessory enzymes such as xylanase: is it an additive or synergistic effect? Biotechnology for Biofuels 2011:4:36.
10. Leu S-Y, Zhu JY. Substrate-Related Factors Affecting Enzymatic Saccharification of Lignocelluloses: Our Recent Understanding. Bioenerg Res. 2012;6(2):405-15.
11. Zhang Y, Culhaoglu T, Pollet B, Melin C, Denoue D, Barriere Y, et al. Impact of Lignin Structure and Cell Wall Reticulation on Maize Cell Wall Degradability. Journal of Agricultural and Food Chemistry. 2011;59(18):10129-35.
12. Kumar R, Wyman CE. Key features of pretreated lignocelluloses biomass solids and their impact on hydrolysis. 2010:73-121.
13. Hall M, Bansal P, Lee JH, Realff MJ, Bommarius AS. Cellulose crystallinity–a key predictor of the enzymatic hydrolysis rate. FEBS J. 2010;277(6):1571-82.
14. Sinitsyn AP, Gusakov AV, Vlasenko EY. Effect of structural and physicochemical features of cellulosic substrates on the efficiency of enzymatic hydrolysis Applied Biochemistry and Biotechnology. 1991;30(1):43-59.
15. Grethlein HE. The effect of pore size distribution on the rate of enzymatic hydrolysis of cellulosic substrates. Bio-Technology. 1985;3(2):155-60.
16. Meng X, Pu Y, Yoo CG, Li M, Bali G, Park DY, et al. An In-Depth Understanding of Biomass Recalcitrance Using Natural Poplar Variants as the Feedstock. ChemSusChem. 2017;10(1):139-50.
17. Marriott PE, Gomez LD, McQueen-Mason SJ. Unlocking the potential of lignocellulosic biomass through plant science. New Phytol. 2016;209(4):1366-81.
18. Silva GGD, Couturier M, Berrin J-G, Buléon A, Rouau X. Effects of grinding processes on enzymatic degradation of wheat straw. Bioresource Technology. 2012;103(1):192-200.
19. Vidal BC, Dien BS, Ting KC, Singh V. Influence of feedstock particle size on lignocellulose conversion—A Review. Applied Biochemistry and Biotechnology. 2011;164(8):1405-21.
20. Grethlein HE, Converse A. Common aspects of acid prehydrolysis and steam explosion for pretreating wood. Bioresource Technology. 1991;36:77-82.
21. Huang R, Su R, Qi W, He Z. Understanding the key factors for enzymatic conversion of pretreated lignocellulose by partial least square analysis. Biotechnol Prog. 2010;26(2):384-92.

22. Thompson DN, Chen HC, Grethlein HE. Comparison of pretreatment methods on the basis of available surface area. Bioresource Technology. 1992;39:155-63.
23. Wong KKY, Deverell KF, Mackie KL, Clark TA, Donaldson LA. The relationship between fiber porosity and cellulose digestibility in steam exploded pinus radiata. Biotechnology and Bioengineering. 1988;31:447-56.
24. Chandra RP, Ewanick SM, Chung PA, Au-Yeung K, Del Rio L, Mabee W, et al. Comparison of methods to assess the enzyme accessibility and hydrolysis of pretreated lignocellulosic substrates. Biotechnology letters. 2009;31(8):1217-22.
25. Chandra RP, Ewanick SM, Hsieh C, Saddler JN. The characterization of pretreated lignocellulosic substrates prior to enzymatic hydrolysis, Part 1: A modified Simons' staining technique. Biotechnol Prog 2008;24:1178-85.
26. Meng X, Foston M, Leisen J, DeMartini J, Wyman CE, Ragauskas AJ. Determination of porosity of lignocellulosic biomass before and after pretreatment by using Simons' stain and NMR techniques. Bioresource Technology. 2013;144:467-76.
27. Forsström J, Andreasson B, Wagberg L. Influence of pore structure and water retaining ability of fibres on the strength of papers from unbleached kraft fibres. Nordic Pulp and Paper Research Journal. 2005;20(2):176-85.
28. Li M, Heckwolf M, Crowe JD, Williams DL, Magee TD, Kaeppler SM, et al. Cell-wall properties contributing to improved deconstruction by alkaline pre-treatment and enzymatic hydrolysis in diverse maize (Zea maysL.) lines. Journal of Experimental Botany. 2015;66(14):4305-15.
29. Weiss ND, Felby C, Thygesen LG. Enzymatic hydrolysis is limited by biomass-water interactions at high-solids: improved performance through substrate modifications. Biotechnol Biofuels. 2019;12:3.
30. Weiss ND, Thygesen LG, Felby C, Roslander C, Gourlay K. Biomass-water interactions correlate to recalcitrance and are intensified by pretreatment: An investigation of water constraint and retention in pretreated spruce using low field NMR and water retention value techniques. Biotechnol Prog. 2017;33(1):146-53.
31. Williams DL, Hodge DB. Impacts of delignification and hot water pretreatment on the water induced cell wall swelling behavior of grasses and its relation to cellulolytic enzyme hydrolysis and binding. Cellulose. 2014;21(1):221-35.
32. Meng X, Ragauskas AJ. Recent advances in understanding the role of cellulose accessibility in enzymatic hydrolysis of lignocellulosic substrates. Current opinion in biotechnology. 2014;27:150-8.
33. Weiss ND, Felby C, Thygesen LG. Water retention value predicts biomass recalcitrance for pretreated lignocellulosic materials across feedstocks and pretreatment methods. Cellulose. 2018;25(6):3423-34.
34. Anderson WF, Akin DE. Structural and chemical properties of grass lignocelluloses related to conversion for biofuels. Journal of Industrial Microbiology & Biotechnology. 2008;35(5):355-66.
35. Chabbert B, Habrant A, Herbaut M, Foulon L, Aguie-Beghin V, Garajova S, et al. Action of lytic polysaccharide monooxygenase on plant tissue is governed by cellular type. Sci Rep. 2017;7(1):17792.
36. Devaux M-F, Jamme F, André W, Bouchet B, Alvarado C, Durand S, et al. Synchrotron Time-Lapse Imaging of Lignocellulosic Biomass Hydrolysis: Tracking Enzyme Localization by Protein Autofluorescence and Biochemical Modification of Cell Walls by Microfluidic Infrared Microspectroscopy. Frontiers in Plant Science. 2018;9.
37. Ding SY, Liu YS, Zeng Y, Himmel ME, Baker JO, Bayer EA. How does plant cell wall nanoscale architecture correlate with enzymatic digestibility? Science. 2012;338:1055-60.
38. Belmokhtar N, Habrant A, Lopes Ferreira N, Chabbert B. Changes in Phenolics Distribution After Chemical Pretreatment and Enzymatic Conversion of Miscanthus × giganteus Internode. Bioenerg Res. 2013;6(2):506-18.
39. Lopez S, Murison SD, Travis AJ, Chesson A. Degradability of parenchyma and sclerenchyma cell walls isolated at different developmental stages from a newly extended maize internode. Acta Bot Neerl. 1993;42(2):165-74.
40. Wilson JR, Mertens DR, Hatfield RD. Isolates of cell-types from sorghum stems - Digestion, cell-wall and anatomical characteristics J Sci Food Agric. 1993;63(4):407-17.
41. Jin SY, Chen HZ. Fractionation of fibrous fraction from steam-exploded rice straw. Process Biochemistry. 2007;42(2):188-92.
42. Papatheofanous MG, Billa E, Koullas DP, Monties B, Koukios EG. Optimizing multisteps mechanical-chemical fractionation of wheat straw components. Industrial Crops and Products. 1998;7(2-3):249-56.
43. Mayer-Laigle C, Barakat A, Barron C, Delenne JY, Frank X, Mabille F, et al. DRY biorefineries: Multiscale modeling studies and innovative processing. Innovative Food Science & Emerging Technologies. 2018;46:131-9.
44. Bootsma JA, Shanks BH. Hydrolysis characteristics of tissue fractions resulting from mechanical separation of corn stover. Applied Biochemistry and Biotechnology. 2005;125:27-39.
45. Chundawat SPS, Venkatesh B, Dale BE. Effect of particle size based separation of milled corn stover on AFEX pretreatment and enzymatic digestibility. Biotechnology and Bioengineering. 2007;96(2):219-31.

46. Barakat A, Mayer-Laigle C. Electrostatic separation as an entry into environmentally eco-friendly dry biorefining of plant materials. Journal of Chemical Engineering & Process Technology. 2017;08(04).
47. Williams MW. Triboelectring charging of insulating polymers - some new perspectives. AIP Advances. 2012;2(1).
48. Morrison TA, Jung HG, Buxton DR, Hatfield RD. Cell-wall composition of maize internodes of varying maturity. Crop Science. 1998;38(2):455-60.
49. Jones RW, Krull LH, Blessin CW, Inglett GE. Neutral sugars of hemicellulose fraction of pith from stalk of selected plants. Cereal Chemistry. 1979;56(5):441-2.
50. McKinley BA, Olson SN, Ritter KB, Herb DW, Karlen SD, Lu F, et al. Variation in energy sorghum hybrid TX08001 biomass composition and lignin chemistry during development under irrigated and non-irrigated field conditions. PLoS One. 2018;13(4):e0195863.
51. Duguid KB, Montross MD, Radtke CW, Crofcheck CL, Wendt LM, Shearer SA. Effect of anatomical fractionation on the enzymatic hydrolysis of acid and alkaline pretreated corn stover. Bioresource Technology. 2009;100(21):5189-95.
52. Hodgson-Kratky K, Papa G, Rodriguez A, Stavila V, Simmons B, Botha F, et al. Relationship between sugarcane culm and leaf biomass composition and saccharification efficiency. Biotechnol Biofuels. 2019;12:247.
53. Akin DE, Hartley RD. Microspectrophotometry and digestibility of alkali-treated walls in bermudgrass cell-types. Crop Science. 1992;32(5):1116-22.
54. Soille P. Morphological image compositing. EEE TRANSACTIONS ON PATTERN ANALYSIS AND MACHINE INTELLIGENCE. 2006;28(5):673-83.
55. Mansfield SD, Mooney C, Saddler JN. Substrate and enzyme characteristics that limit cellulose hydrolysis. Biotechnol Prog. 1999;15:804-16.
56. Montross MD, Crofcheck CL. Effect of stover fraction and storage method on glucose production during enzymatic hydrolysis. Bioresource Technology. 2004;92(3):269-74.
57. Tanaka M, Ikesaka M, Matsuno R, Converse A. Effect of Pore Size in Substrate and Diffusion of Enzyme on Hydrolysis of Cellulosic Materials with Cellulases. Biotechnolgy and Bioengineering. 1988;32:698-706.
58. Lahaye M, Falourd X, Limami AM, Foucat L. Water Mobility and Microstructure Evolution in the Germinating Medicago truncatula Seed Studied by NMR Relaxometry. A Revisited Interpretation of Multicomponent Relaxation. Journal of Agricultural and Food Chemistry. 2015;63(6):1698-710.
59. Kuniak L, Marchessault RH. Study of the crosslinking reaction between epichlorohydrin and starch. Dis Stärke. 1972;24(4):110:6.
60. Guillon F, Auffret A, Robertson JA, Thibault JF, Barry JL. Relationships between physical characteristics of sugar-beet fibre and its fermentability by human faecal flora. Carbohydrate Polymers. 1998; 37:185–97.
61. Berman P, Levi O, Parmet Y, Saunders M, Wiesman Z. Laplace Inversion of Low-Resolution NMR Relaxometry Data Using Sparse Representation Methods. Concepts Magn Reson Part A Bridg Educ Res. 2013;42(3):72-88.
62. Saunders M. PDCO: primal–dual interior method for convex objectives. http://web.stanford.edu/group /SOL/softw are/pdco/. Accessed Jan 2017.2017.
63. Timpano H, Sibout R, Devaux M-F, Alvarado C, Looten R, Falourd X, et al. Brachypodium cell wall mutant with enhanced saccharification potential despite increased lignin content. Bioenerg Res. 2014;8(1):53-67.
64. Tollier MT, Robin JP. Adaptation de la méthode à l'orcinol-sulfurique au dosage automatique des glucides neutres totaux: conditions d'application aux extraits d'origine végétale. Ann Technol Agric. 1979;28(1):1-15.
65. Thibault JF. Automatisation du dosage des substances pectiques par la méthode au metahydroxyphenyl. 1979.
66. Levigne S, Thomas M, Ralet MC, Quemener B, Thibault JF. Determination of the degrees of methylation and acetylation of pectins using a C18 column and internal standards. Food Hydrocolloids. 2002;16(6):547-50.
67. Antoine C, Peyron S, Mabille F, Lapierre C, Bouchet B, Abecassis J, et al. Individual contribution of grain outer layers and their cell wall structure to the mechanical properties of wheat bran. Journal of Agricultural and Food Chemistry. 2003;51(7):2026-33.
68. Dence CW. The determination of lignin. In: Lin SY, Dence CW, editors. Methods in lignin chemistry. Berlin, Germany: Springer-Verlag; 1992. p. 33-61.
69. Lapierre C, Pollet B, Petit-Conil M, Toval G, Romero J, Pilate G, et al. Structural Alterations of Lignins in Transgenic Poplars with Depressed Cinnamyl Alcohol Dehydrogenase or Caffeic Acid O-Methyltransferase Activity Have an Opposite Impact on the Efficiency of Industrial Kraft Pulping. Plant Physiology and Biochemistry. 1999;119:153-63.
70. Devaux MF, Taralova I, Levy-Vehel J, Bonnin E, Thibault JF, Guillon F. Contribution of image analysis to the description of enzymatic degradation kinetics for particulate food material. Journal of Food Engineering. 2006;77(4):1096-107.

71. Devaux MF, Legland D. Grey level granulometry for histological image analysis of plant tissues. In: Méndez-Vilas A, editor. Microscopy: advances in scientific research and education: Formatex Research Center; 2014. p. 681-8.

Tables

Table 1. Yield of maize shoot fractions and physical characteristics of maize shoot powder and its fractions.

Sample	Yield	D_{50}	Span	Ssp
	(% dm)	(µm)		($m^2.g^{-1}$)
M		171.3	2.9	0.97
M*c*-	18.5	315.6	1.9	0.60
M*c*+	24.5	309.5	2.0	0.59
M*m*-	11.7	201.4	2.1	0.87
M*m*+	10.3	159.1	2.4	0.79
M*f*-	18.6	62.8	2.4	1.51
M*f*+	16.5	58.0	2.0	1.80

D_{50}: median particle diameter, span: $(D_{90}-D_{10})/D_{50}$, Ssp: specific surface area

Table 2. Chemical composition of maize shoot powder and its fractions

Sample	sugars (% dm)						Ash	Proteins	Acetyls	lignin			CA	FA
	Total	Ara	Xyl	Glu	Gal	Uronic acids	(%dm)	(% dm)	(% dm)	Klason Lignin (% dm)	Thio yield (µmol.g^{-1} KL)	S/G	(mg.g^{-1} dm)	(mg.g^{-1} dm)
M	66.3	2.8	20.6	38.1	1.0	3.4	3.58	3.48	4.74	18.50	777.5	1.04	17.24	6.19
M*c*-	67.2	2.7	22.1	38.0	0.8	3.2	2.61	2.17	3.75	19.01	823.5	0.92	19.00	6.79
M*c*+	68.2	2.5	22.4	39.0	0.8	3.2	2.10	2.20	5.05	19.56	999.0	1.00	20.41	6.79
M*m*-	67.6	3.4	22.3	37.1	1.1	3.3	4.01	2.42	3.98	14.79	748.5	0.90	12.54	5.19
M*m*+	65.7	2.6	20.1	38.4	0.9	3.2	2.42	4.41	4.25	16.58	828.5	1.08	15.87	6.03
M*f*-	67.3	3.6	19.8	37.6	1.4	4.3	3.38	3.70	4.06	15.43	720.5	1.28	15.37	5.70
M*f*+	64.7	2.9	17.9	37.9	1.1	4.3	1.85	4.56	4.84	14.52	918.5	1.42	20.28	6.49

Ara: arabinose, Xyl: xylose, Glu: glucose, Gal: galactose, Klason lignin: expressed according to the dry matter of the extractive free material, Thio yield: expressed according to the amount of klason lignin (KL), CA: ester-linked *p*-coumaric acid, FA: ester-linked ferulic acid, dm: dry matter.

Table 3. Water interaction properties of maize shoot powder and its fractions.

Sample	Swelling Capacity	Water Retention Capacity
	($mL.g^{-1}$)	($g.g^{-1}$)
M	7.5	8.25
M*c-*	5.0	5.60
M*c+*	5.0	5.55
M*m-*	6.0	7.15
M*m+*	6.0	6.90
M*f-*	7.5	8.85
M*f+*	9.0	8.00

Figures

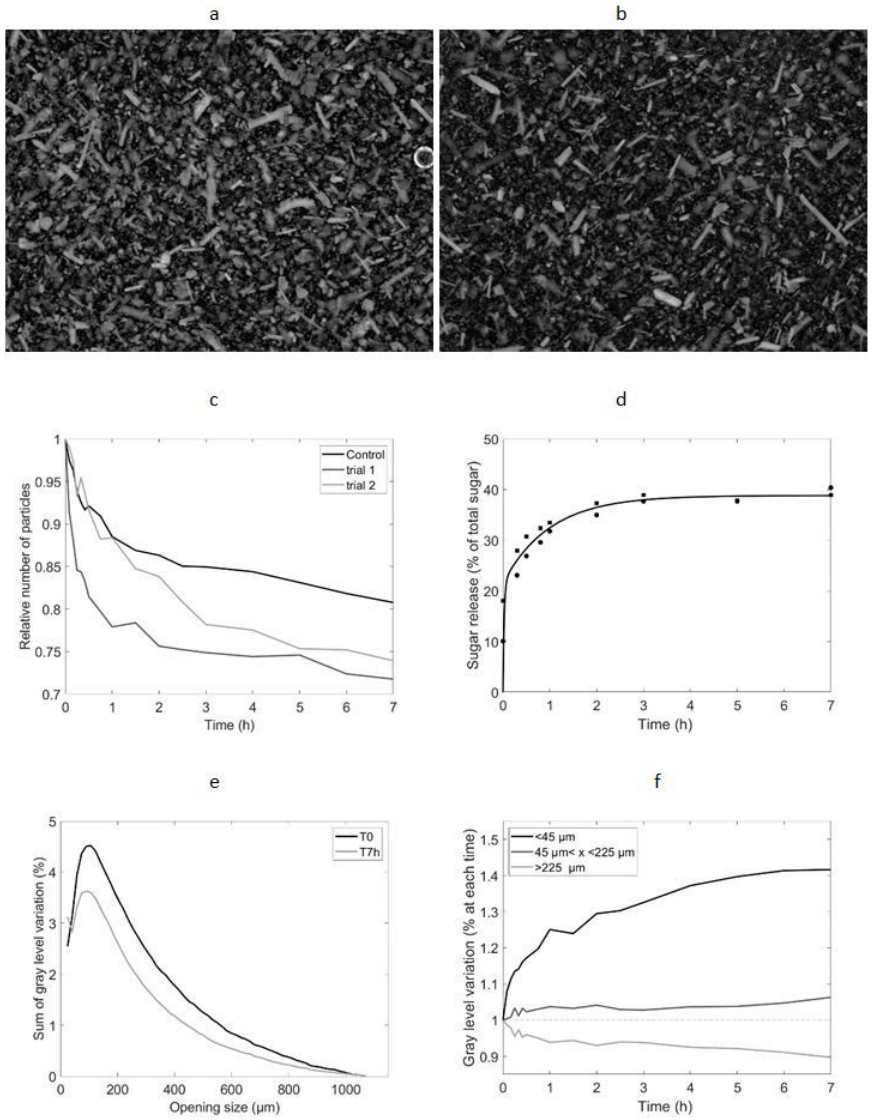

Figure 1

Saccharification of maize powder in the torus reactor Cinetore. a) picture of the original sample b) picture of the sample after 7 h of saccharification. Field of view: 10x13.3 mm^2. c) Changes in the relative number of particles measured as the sum of gray levels relative to time T0 in the control experiment and two enzymatic degradation trials. d) Percentage of sugar released according to hydrolysis time. e) Granulometric curves of the original sample and after 7 h saccharification. M – T0: time T0 normalized to 1, M – T7 h: time 7 h normalized to

1, M – 7 h norm T0: time 7 h normalized relatively to the amount of particles at time T0. f) Changes in the three classes of particles relative to their original number.

Figure 2

Optical observation of fractions of maize shoot powder: A) Mf+, B) Mf-, C) Mm+, D) Mm-, E) Mc+, F) Mc- (the bar scale represents 500 µm).

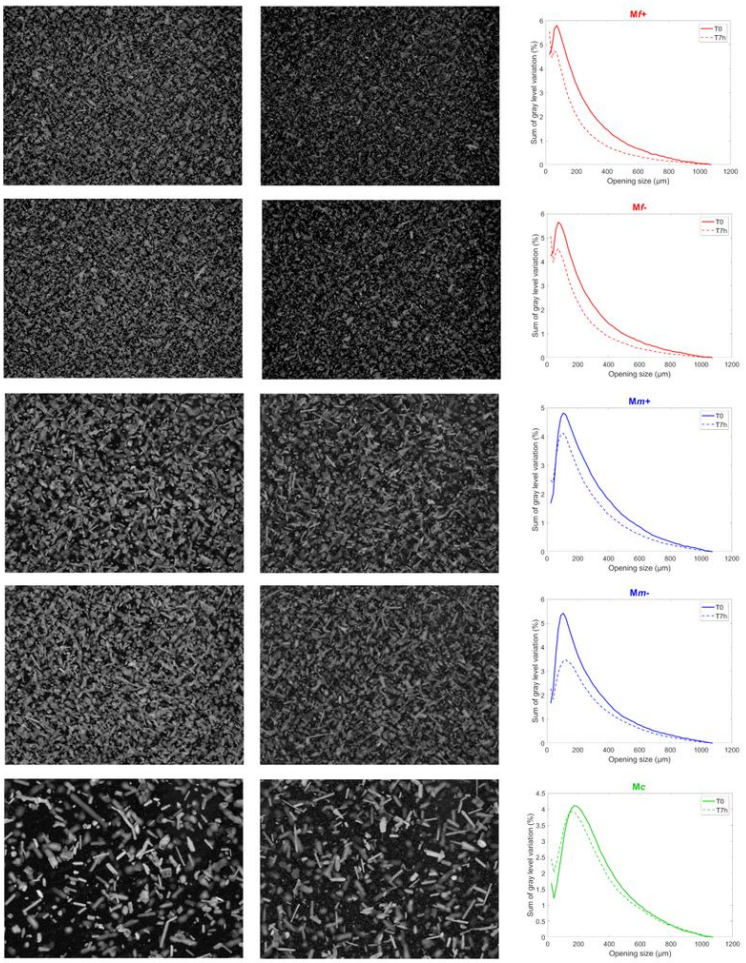

Figure 3

Cinetore Analysis. Examples of image at times 0 and 7 hours for maize shoot fractions: from top to bottom: Mf+, Mf-, Mm+, Mm- and Mc. Field of view: 10.0x13.3 mm². Brightness and contrast were set at 60 and -40 for the fine fractions and to 40 and -40, respectively for the three other fractions. Granulometric curves of the original sample and after 7 h saccharification. T0: time T0 normalized to 1, T7h: time 7 h normalized relative to the number of particles at time T0

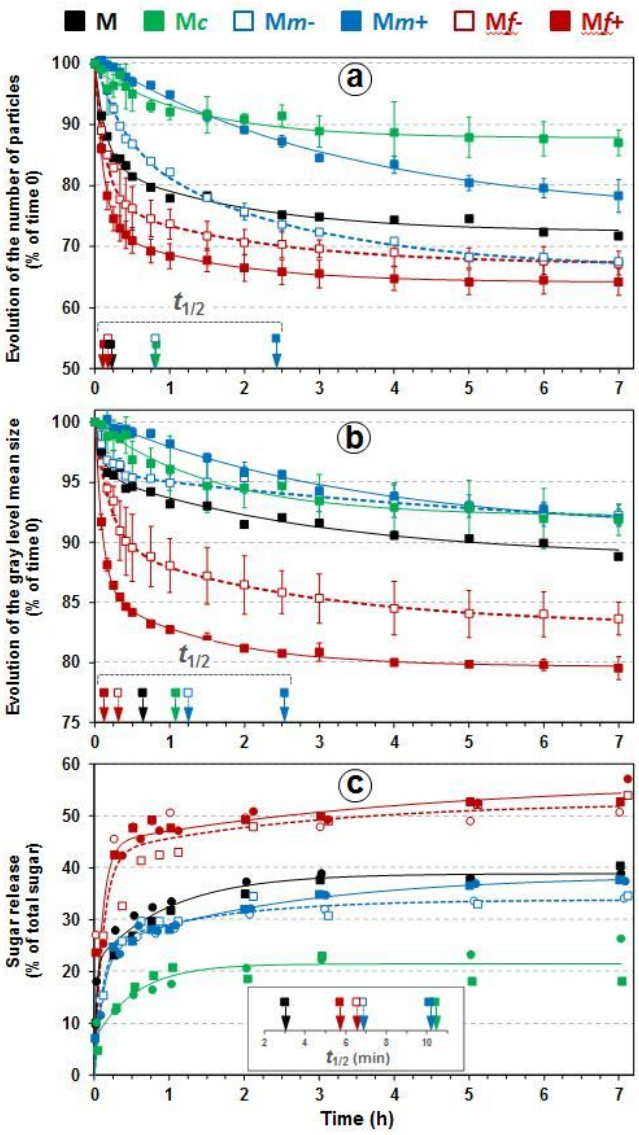

Figure 4

Kinetics of saccharification of maize shoot fractions (M, Mc, Mm+, Mm-, Mf+ and Mf-), in the reactor CINETORE. A) Changes in the number of particles over time T0, B) Changes in the mean particle size relative to time T0, C) Sugar release (% of total sugars).

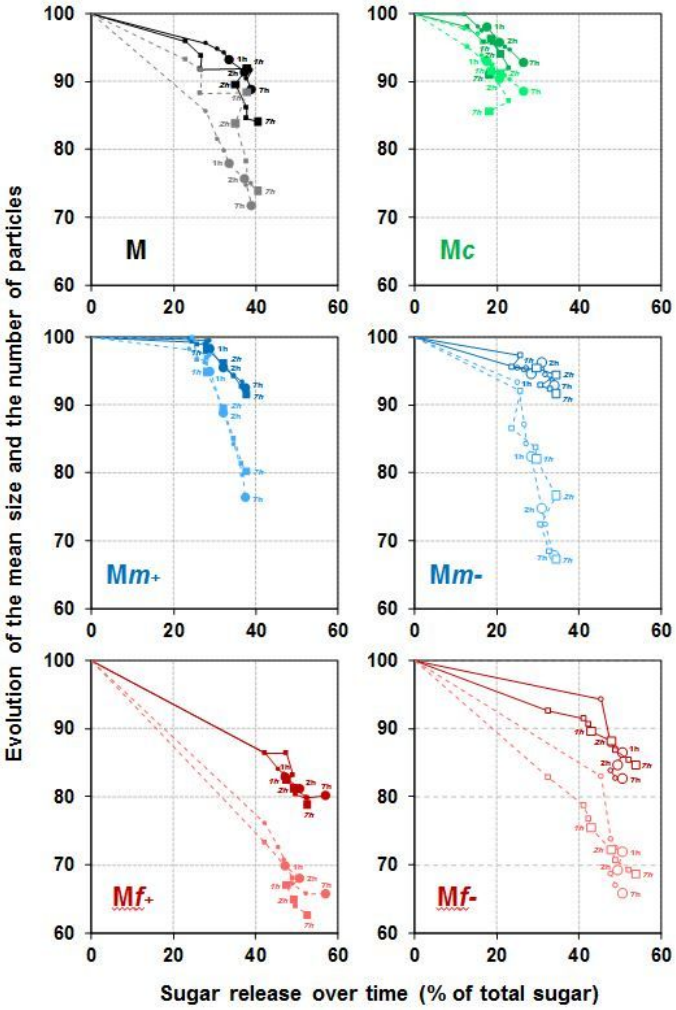

Figure 5

Saccharification of maize shoot fractions in the reactor CINETORE. Changes in the relative mean particle size (solid line) and relative number of particles (dotted lines) according to the relative percentage of neutral sugars released through enzymatic hydrolysis in fractions M, Mc, Mm+, Mm-, Mf+ and Mf-. Each point corresponds to different hydrolysis times (15 min, 30 min, 45 min 1 h, 2 h, 3 h, 5 h, 7 h

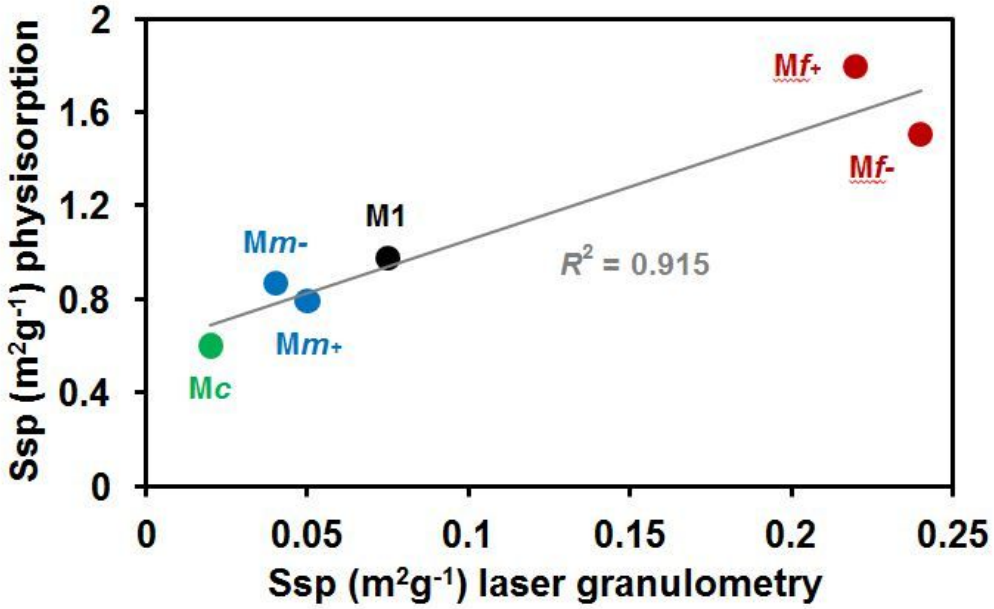

Figure 6

Specific surface area of maize shoot fractions according to the method of evaluation used.

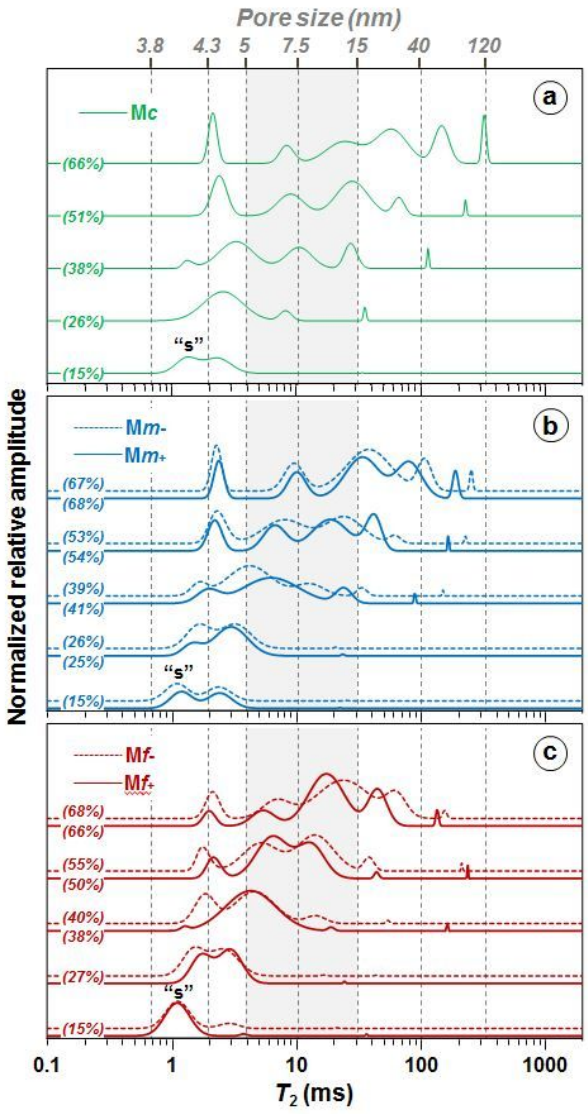

Figure 7

LF-NMR T2 distributions for coarse (a), medium (b) and fine (c) fractions with increasing water content. The x-axis is logarithmic scale, and distribution amplitude is expressed in normalized relative water content (% w/w). The letter "s" denotes the shortest T2 component (T2s) at 15% MC. The correspondence (vertical dashed lines) between meso porosity (in nm) and T2 relaxation times is indicated at the top of the Figure. The shaded area, between 5 nm and 15 nm (associated with T2 values centered around 4 ms and 30 ms, respectively), indicate the range of pore sizes available for enzyme accessibility.

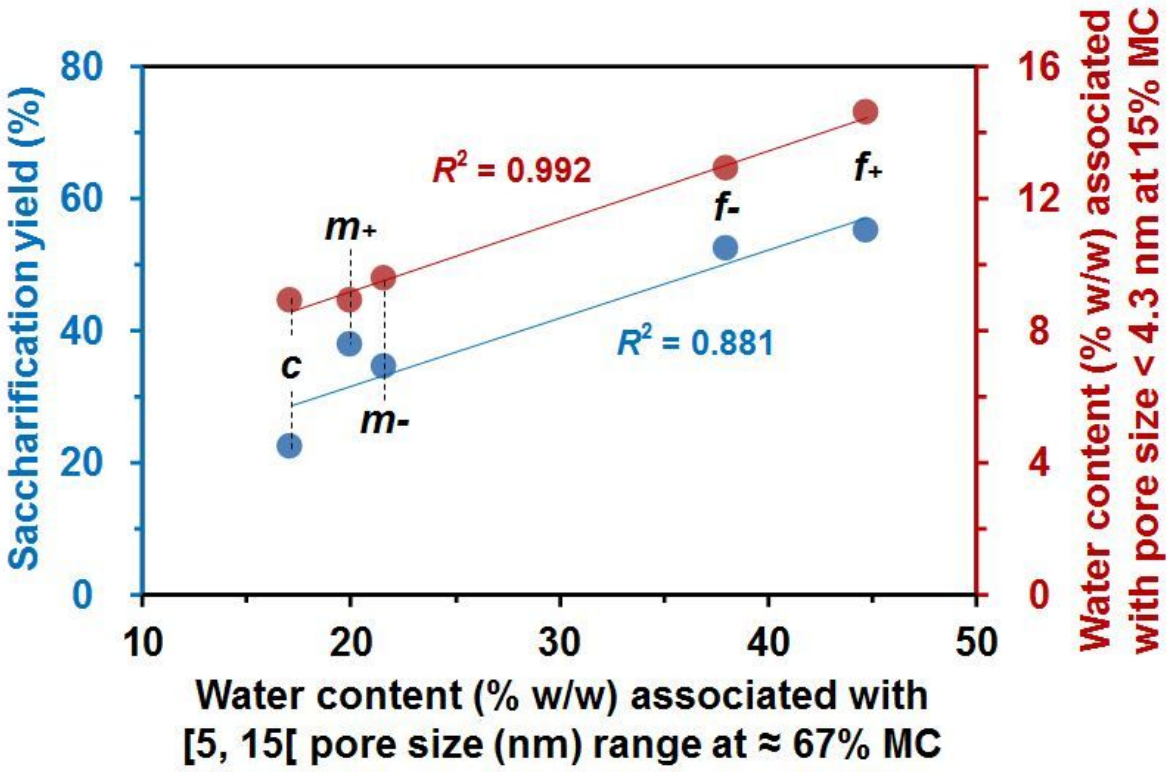

Figure 8

Inter-relationships between saccharification yield and water content associated with [5, 15[pore size range (in nm), relative to the shaded area in Figure 8, at 15% and 67% MC.

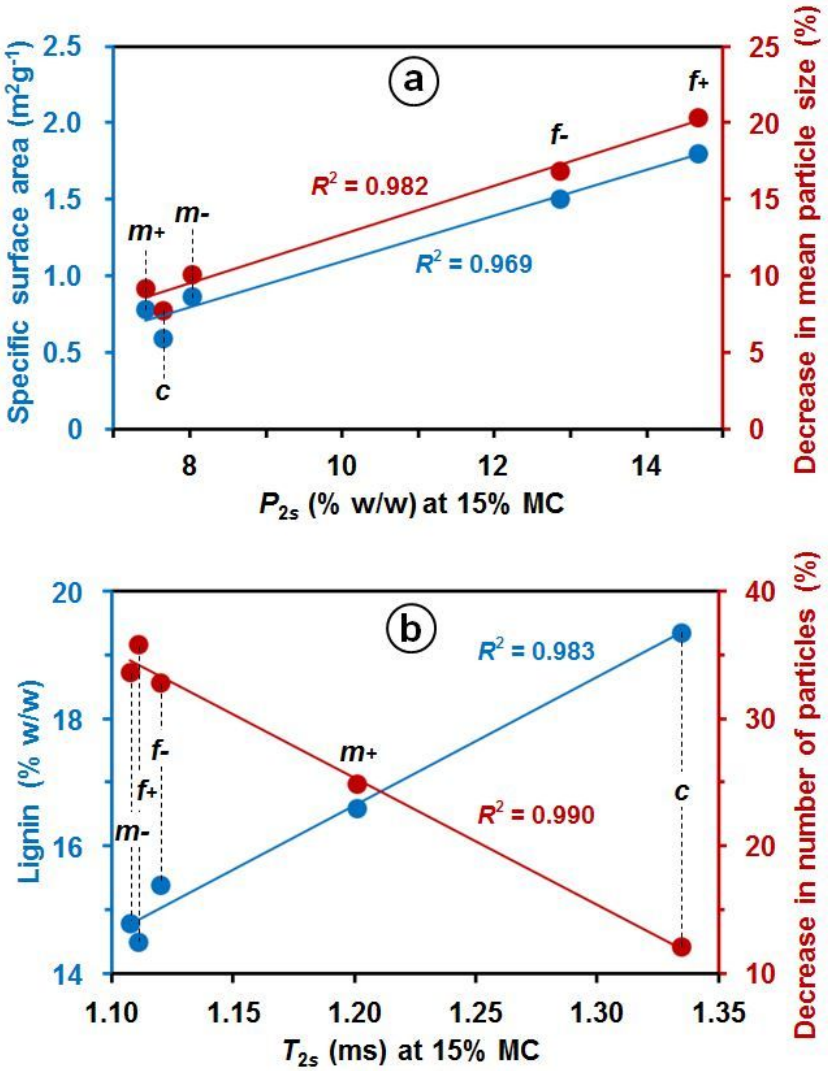

Figure 9

Inter-relationships between specific physicochemical characteristics ((a) lignin content and reduction in the number of particles; (b) Ssp (specific surface area) and reduction in particle mean size and the NMR relaxation parameters associated with the shortest T2 component “s”: (a) T2s and (b) P2s.

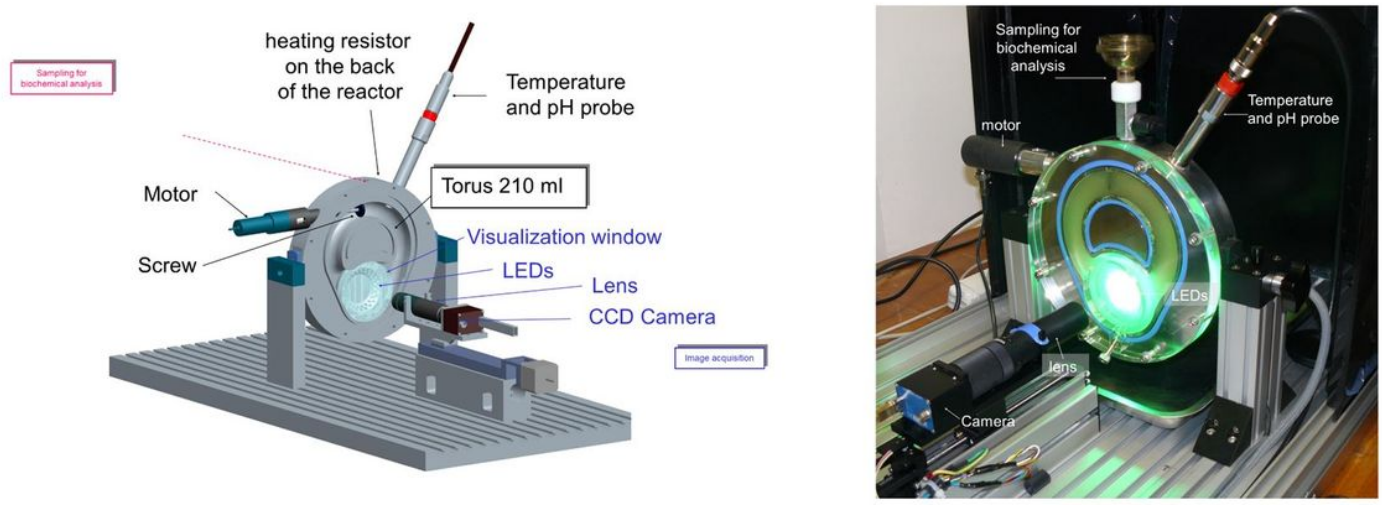

Figure 10

The torus reactor CINETORE. Scheme and photograph.

Supplementary Files

This is a list of supplementary files associated with this preprint. Click to download.

- Additionalfile2.pdf
- Additionalfile1.docx